

Analysis and Modeling GPS NLOS effect in Highly Urbanized Area

Li-Ta Hsu

Interdisciplinary Division of Aeronautical and Aviation Engineering, The Hong Kong
Polytechnic University, Hong Kong

ABSTRACT

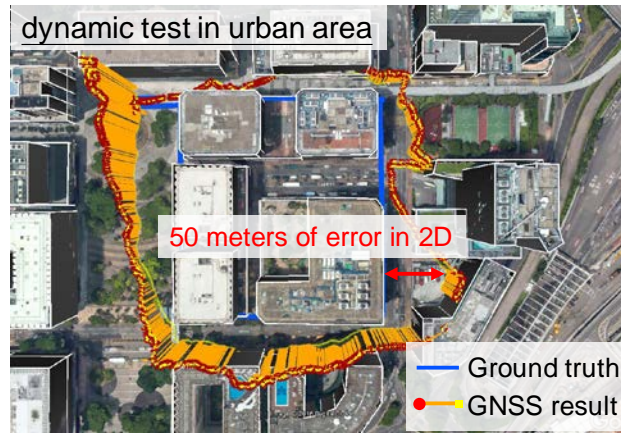
Current GPS positioning accuracy in urban areas is still unsatisfactory for various applications, including pedestrian navigation and autonomous driving. Due to the ineffectiveness of special corrector designs against non-line-of-sight (NLOS) reception, the research regarding NLOS signals has been increasing in the recent years. This study first develops an algorithm to detect NLOS signals from the pseudorange measurements by using a 3D building model, ray-tracing simulation, and known receiver position. According to the analysis of 24 hours of collected NLOS data, a new finding is that NLOS pseudorange delay is highly correlated with the elevation angle of satellite instead of the received signal strength. Thus, we further propose an innovative NLOS model using two variables, the elevation angle and the distance between the receiver and building that reflect the NLOS. The proposed model is evaluated in both pseudorange and position domains. Based on the experiment results regarding pseudorange error, the difference between the proposed model and the collected NLOS measurement is very small. Finally, the proposed model is applied to a hypothesis based positioning method and achieves about 6.3 meters in terms of horizontal positioning accuracy, which is only slightly worse than the method applied with ray-tracing simulation.

Introduction

The booming of transportation robotics such as unmanned aerial vehicle (UAV) and driverless car pushes the requirement of accuracy and precision of low-cost global navigation satellite system (GNSS) receivers. Multipath and non-line-of-sight (NLOS) receptions still are the main challenges for GNSS receiver in urban canyon (Groves 2013). Especially in Asian super urbanized cities such as Hong Kong and Tokyo, the challenges from the signal reflection at the dense skyscrapers further increasing the difficulty. Figure 1 shows the positioning data calculated

30 by a commercial GNSS receiver, u-blox M8 receiver (GPS/Beidou mode), and collected in
31 Kowloon, HK. Comparing the top and bottom panels of the figure, the positioning accuracy in
32 urban area is much worse than that in the open area. It is evident the poor GNSS positioning
33 result is caused by the GNSS signal blockage and reflection from the surrounding buildings.

34



35



36

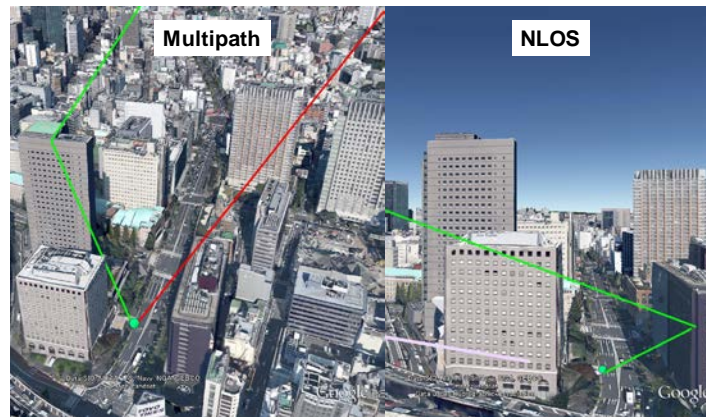
37 **Fig. 1** Performance of a low-cost GNSS receiver obtained dynamically and statically from a
38 quadcopter in the urban and open area of Kowloon, HK, respectively, on September, 2016.

39

40 Multipath and NLOS are different effects (Groves 2013), which are shown in Figure 2.
41 Multipath contains both the direct and reflected signals while NLOS contains only the latter one.
42 Even for a low-cost GNSS receiver, the multipath effect can be mitigated by sophisticated
43 receiver correlator designs (Veitsel et al. 1998; Zhdanov et al. 2002). The principle of the
44 correlator design is comparing the early, prompt and late channels in code tracking loop. In the

45 other words, it compares the direct signal with reflected one. Unfortunately, this design does not
46 mitigate the NLOS effect at all because the NLOS contains only the reflected signal. Thus, the
47 research focused on detection and mitigation of NLOS is increasing. Detecting the NLOS using
48 carrier to noise ratio (C/N_0) measurements of dual-polarization antenna is discussed in Jiang and
49 Groves (2014). An advance tracking algorithm, i.e. vector tracking, has been proposed to detect
50 and mitigate NLOS effect in signal processing stage (Benson 2007; Hsu et al. 2015; Kanwal
51 2011). Consistency check between pseudorange measurements could detect and exclude large
52 multipath and NLOS effects when the number of clean measurement is sufficient (Blanch et al.
53 2015; Groves and Jiang 2013; Iwase et al. 2013; Hsu et al. 2017). Another direction of study is to
54 add other sensors to compensate the inaccurate GNSS positioning result caused by NLOS effect
55 (Chiang et al. 2013; Gu et al. 2015; Han et al. 2015; Li et al. 2015; Sun et al. 2013; Wang and
56 Gao 2010).

57



58

59 **Fig. 2** Illustration of signal reception of multipath and NLOS effects (Hsu et al. 2016b).

60

61 Due to the rise of smart cities, the 3D city models are rapidly developed and became widely
62 available. Recent research dealing with multipath and NLOS utilizes 3D mapping and is called
63 as 3D mapping aided (3DMA) positioning methods. Comprehensive related work on 3DMA
64 positioning method can be found at Groves et al. (2015) and Breßler et al. (2016). One of the
65 most well-known 3DMA methods is shadow matching proposed by university college London
66 (UCL). It takes advantage of the 3D city model to generate building boundary in the skyplot to
67 help predicting satellite visibility (Groves 2011; Wang et al. 2012; Wang et al. 2013; Wang et al.

68 2015). The improvements of shadow matching in land, aviation, and mapping applications are
69 deeply investigated by American and Israeli researchers (Yozevitch et al. 2014; Isaacs et al.
70 2014; Yozevitch and Ben-Moshe 2015). Researchers from the French institute of science and
71 technology for transport (IFSTTAR) and the national higher French institute of aeronautics and
72 space (ISAE-SUPAERO) also focused on improved GNSS positioning accuracy using enhanced
73 3D digital map (Ahmad et al. 2013; Betaille et al. 2013; Peyraud et al. 2013; Peyret et al. 2014).
74 Instead of mitigating or excluding NLOS effect, in the past three years the potential of using
75 NLOS signal in constructive senses has been proposed. Researchers from Japan and Canada
76 propose to combine ray-tracing simulation with hypothesis-based positioning method to further
77 improve the positioning accuracy (Hsu et al. 2016b; Kumar and Petovello 2014; Miura et al.
78 2015; Suzuki and Kubo 2013). The range-based 3DMA uses a ray-tracing technique to estimate
79 the reflection route of NLOS signal. The route is then used to correct the NLOS delay from the
80 biased pseudorange measurement and it further improves positioning accuracy to about 5 meters
81 for pedestrian applications (Hsu et al. 2016a). However, the range-based method cannot be easily
82 adapted to low-cost receiver due to 1) the heavy computational load caused by ray-tracing and 2)
83 the inaccessibility to 3D building models in real-time. The novelty and contribution of this
84 research is to propose a NLOS model that can be used for hypothesis-based positioning without
85 using ray-tracing in the low-cost devices.

86 To achieve the goal, the pseudorange error and its C/N_0 has to be investigated. In the stage
87 of analysis, the NLOS is identified by a given ground truth of the receiver position and by 3D
88 building models. Namely, it is identified if the ray-tracing simulation indicates that the building
89 model obstructs the direct signal transmission path between satellite and receiver, and the
90 receiver still receives it. To obtain the NLOS delay in the pseudorange domain, all the other
91 errors are eliminated using differential GPS (DGPS) correction. 24 Hours of GPS raw data at an
92 highly urbanized area is collected to retrieve the NLOS signals at different C/N_0 from different
93 elevation angle. The result reveals an interesting finding. The pseudorange error caused by
94 NLOS is highly correlated to elevation angle instead of C/N_0 . This finding provides an inside
95 view for modeling NLOS delay as a function of elevation angle and distance from the receiver to
96 the building that reflected the NLOS signal. Note that the distance can be roughly given
97 according to different applications.

98 The detection of NLOS signal and its delay in pseudorange domain is given first. Analysis

99 of 24-hours NLOS data is conducted next, followed by a description of the innovation NLOS
100 pseudorange error model proposed here, and the experimental setup and results. Finally, the
101 conclusions and future work are summarized.

102

103 **Estimation of NLOS Delays in the Pseudorange Domain**

104 NLOS pseudorange measurement deteriorate by delays including tropospheric errors,
105 ionospheric errors, satellite clock/orbit bias, receiver clock bias, and our target NLOS. Other
106 errors must be eliminated before the NLOS analysis. DGPS and least square estimation (LSE)
107 are used to deal with former and latter part of the errors, respectively.

108

109 Differential GPS Correction

110 DGPS is a mature technique (Misra and Enge 2011). A reference station is installed to receive the
111 GPS measurements. The position of the reference station is precisely surveyed. After generating
112 DGPS correction, the correction is transmitted to rover. The rover then applies it to the common
113 satellites in view to enhance its own positioning accuracy. The differential correction can be
114 generated by calculating the difference between the raw pseudorange and true (geometric) range
115 for a satellite. Multipath and NLOS effects to the reference station are usually negligible because
116 the open-sky environment and the geodetic antenna with choke-ring design as shown in the right
117 panel of Figure 3. Theoretically, DGPS correction is capable of eliminating satellite clock/orbit,
118 tropospheric, ionospheric errors if the distance between the reference and rover stations is within
119 100 kilometers. This research uses HKSC station of SatRef, which is a network of GNSS
120 reference stations established by the land department of HK government as shown in Figure 3.
121 The distance between each reference station is less than 20 km. By the use of its archived
122 RINEX 3.02 data that are free to HK publics, the differential correction can be easily generated.

123



124

125 **Fig. 3** Distribution of SatRef stations around HK and antenna and environment of HKSC station.

126

127 Receiver clock bias and thermal noise

128 After applying the DGPS correction to pseudorange measurement, its receiver clock bias and
 129 thermal noise are still required to be corrected. The general LSE uses multiple (at least 4)
 130 measurements to estimate 4 unknowns including horizontal, vertical position and receiver clock
 131 bias as per equation:

$$132 \quad \hat{\mathbf{x}} = \begin{bmatrix} \hat{x} \\ \hat{y} \\ \hat{z} \\ \hat{b} \end{bmatrix} = (\mathbf{G}^T \mathbf{G})^{-1} \mathbf{G}^T \tilde{\boldsymbol{\rho}} \quad (1)$$

133 where $\hat{x}, \hat{y}, \hat{z}$ represent the estimated receiver position in latitude, longitude and altitude
 134 directions and the \hat{b} is the receiver clock bias in meters. \mathbf{G} is the geometry matrix, containing the
 135 unit line-of-sight (LOS) vectors from satellites to receiver. $\tilde{\boldsymbol{\rho}}$ denotes the measured pseudoranges
 136 corrected by DGPS correction. An approach to better estimate the receiver clock bias is to reduce
 137 the unknown $\hat{x}, \hat{y}, \hat{z}$. The receiver is set statically in the experiment so that the ground truth of
 138 receiver position can be easily determined. The ground truth is given by the topographic map
 139 available from land department of HK government. The resolution of the map is 20 centimeters.
 140 Each point is given with accurate 2D coordinate. The height is given by the topography height
 141 obtained from Google plus the height of equipment. Thus, the only unknown left in the LSE is
 142 the receiver clock bias as per equation:

143
$$\hat{\mathbf{b}} = (\mathbf{G}^T \mathbf{G})^{-1} \mathbf{G}^T \tilde{\boldsymbol{\rho}} \quad (2)$$

144 However, if the multipath and NLOS biased measurements are used, the estimated receiver clock
 145 bias will be contaminated. A clean, namely LOS, measurement identification is therefore
 146 required. Two criteria are used to identify the measurement type, and they are the C/N_0 ratio and
 147 the signal type determined by ray-tracing simulation. In general, the C/N_0 of LOS is larger than
 148 that of multipath and NLOS. A 40 dB-Hz threshold of C/N_0 is set empirically. The possible
 149 signal transmission type can be categorized as

150
$$ray \in \{LOS, NLOS\} \quad (3)$$

151 by the use of ray-tracing. The algorithm of rough LOS identification through ray-tracing is as
 152 follows:

153

Algorithm 1: LOS identification for a measurement using ray-tracing simulation	
STEP1:	Prepare a line segment connecting the receiver and the satellite of the measurement (i).
STEP2:	initialize signal type of measurement (i) as LOS, $ray^{(i)} = LOS$
STEP3:	for all the building model \mathbf{B}^j do
STEP3:	for all planes (walls) w_k^j of a building do
STEP4:	if the intersection between the line segment and plane w_k^j exists then
STEP5:	the measurement identified as NLOS, $ray^{(i)} = NLOS$
	break
	end if
STEP6:	end for planes

STEP7: **end for** buildings

154

155 If a measurement has C/N_0 larger than 40 dB-Hz and it is identified as LOS by ray-tracing, the
156 measurement will be used to calculate the receiver clock bias. The receiver thermal noise is
157 neglected because it is much smaller than the effect of NLOS. Finally, the NLOS delay in
158 pseudorange domain, $\Delta\rho_{NLOS}$, can be calculated as,

$$159 \quad \Delta\rho_{NLOS} = \rho - (R^{rcv} + \rho^{corr} + \hat{b}), \quad \forall \rho \in NLOS \quad (4)$$

160 where ρ denotes NLOS pseudorange measurement, R^{rcv} denotes line of sight distance between
161 the satellite and receiver position and ρ^{corr} denotes the DGPS correction. The analysis of the
162 $\Delta\rho_{NLOS}$ is detailed in the next section.

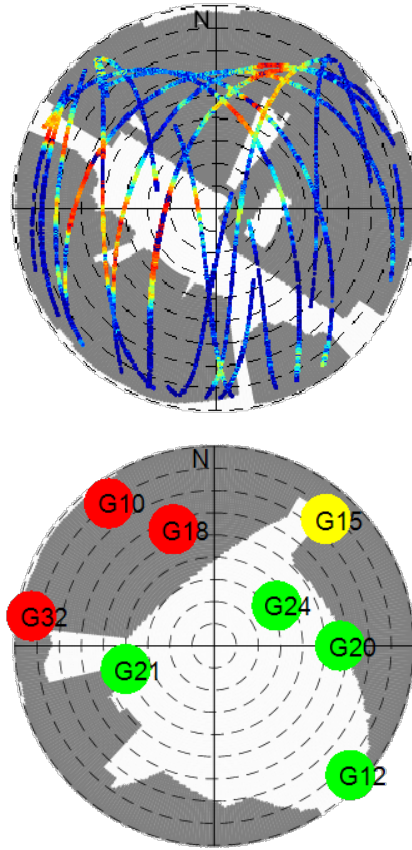
163 The detection of NLOS is simply based on the result of ray-tracing simulation from the
164 given ground truth of receiver position. The NLOS is identified if the LOS path between the
165 satellite and receiver is blocked, but the receiver still receives it.

166

167 **NLOS Data Analysis**

168 Low-cost u-blox M8 receivers are used to record pseudorange measurements. A 3D building
169 model with level of detail (LOD) 1 used in this research is obtained from land department of the
170 HK government. Two data are collected at different locations of urban area of Kowloon, HK.
171 The first and second data consists of 24 hours and 30 minutes of GPS pseudorange
172 measurements, respectively. Figure 4 shows the skyplot of data 1 and 2. As shown in the figure,
173 many signals can be received even if its LOS transmission path is obstructed. In the following
174 analysis, only the identified NLOS signal are evaluated.

175



176

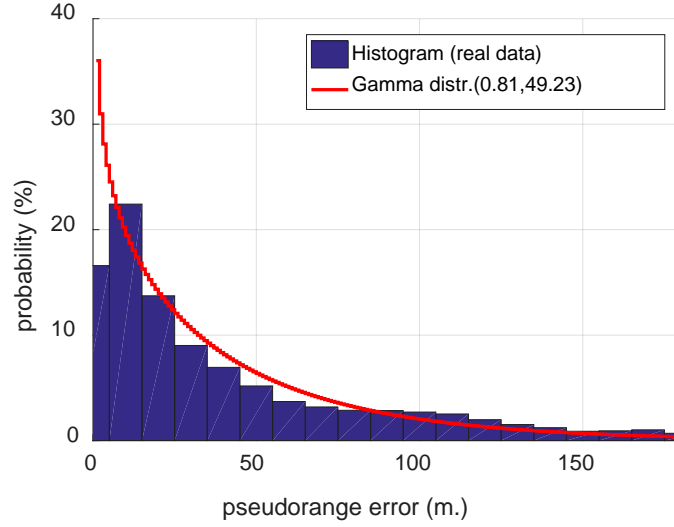
177 **Fig. 4** Skyplots with surrounding building information of data collected in Kowloon. In the top
 178 panel the color of satellite trajectory denotes C/N_0 , the redder the color the higher is the C/N_0
 179 received. In bottom panel green, red and yellow indicate LOS, NLOS and multipath signal
 180 respectively.

181

182 NLOS data 1: Case of 24 hours

183 There are 128,054 NLOS measurements detected in the 24-hours data from different satellites as
 184 demonstrated in the top panel of Figure 4. Figure 5 shows the histogram of NLOS delays in the
 185 pseudorange domain.

186



187

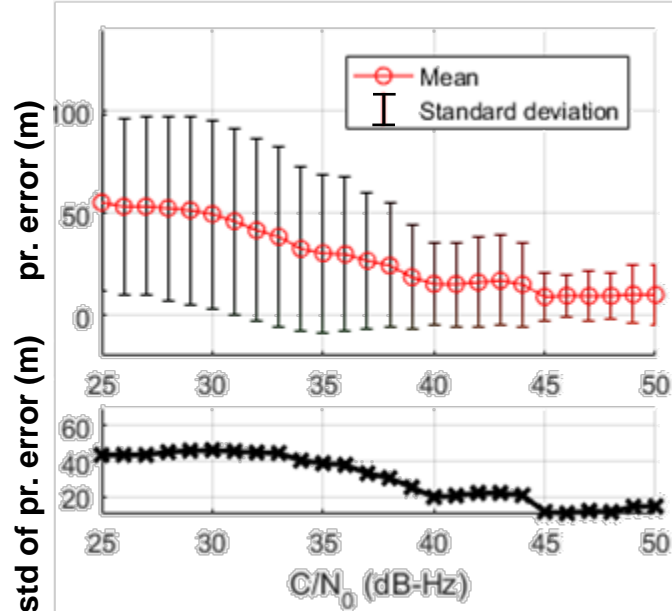
188 **Fig. 5** Histogram of NLOS delays in pseudorange domain. The total number of NLOS signal
 189 received is 128,054.

190

191 The probability density distribution (PDF) of Figure 5 exhibits the probability of an
 192 observed NLOS resulting in a corresponding pseudorange error. As shown in the figure, more
 193 than 70 percent of the NLOS delay is less than 50 meters. Note that this PDF cannot show the
 194 probability of an unknown measurement with a certain pseudorange error to be a NLOS
 195 measurement. It is evident that NLOS delay cannot be modeled as Gaussian distribution. By the
 196 use of maximum likelihood function, the probability density distribution of NLOS delay can be
 197 described as a Gamma distribution:

198
$$f(x|k = 0.81, \theta = 49.23) = \frac{1}{\Gamma(k)\theta^k} x^{k-1} e^{-\frac{x}{\theta}}, \quad (5)$$

199 where $\Gamma(\cdot)$ denotes the Gamma function. Its non-Gaussian property shows the difficulty of
 200 mitigating NLOS effect. As suggested in the popular weighting model, the sigma- ϵ model
 201 (Hartinger and Brunner 1999), the signal strength is a hint to indicate the quality of
 202 pseudorange measurement. Figure 6 shows the relationship between NLOS delay with respect
 203 to C/N_0 . The mean of NLOS error slowly decreases as the C/N_0 increases. Its standard
 204 deviation follows the same trend. This figure roughly verifies the reason that using the sigma- ϵ
 205 model in weighted LSE can improve the GPS positioning result in many cases even in urban
 206 canyon.



208

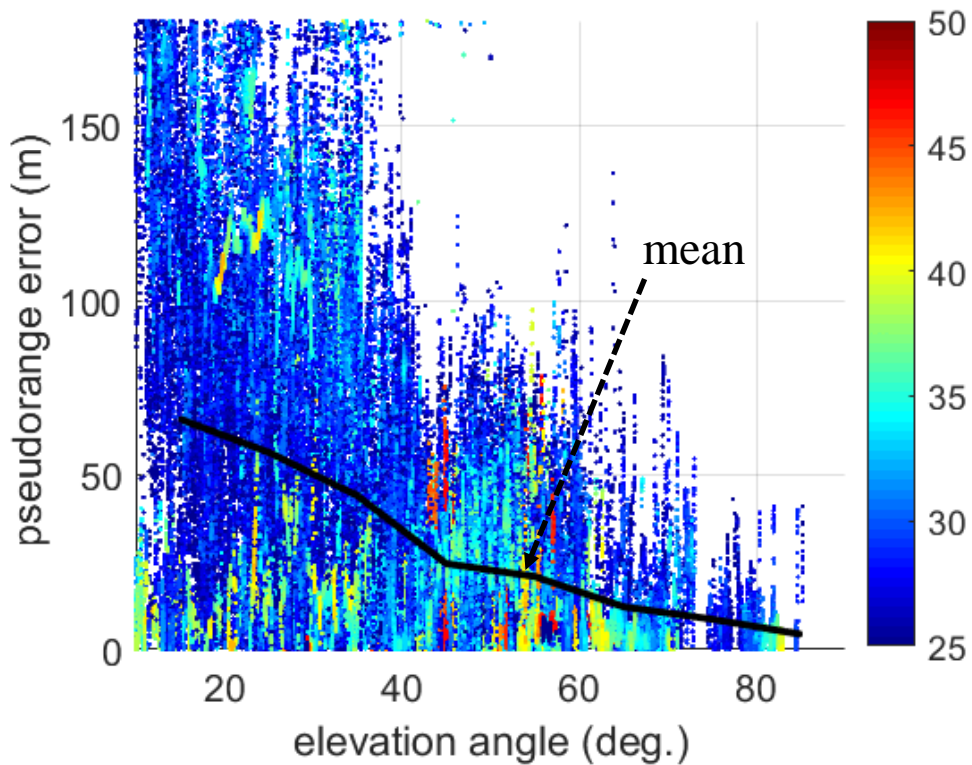
209 **Fig. 6** Mean and standard deviation of NLOS pseudorange error with respect to carrier to noise
 210 ratio.

211

212 Error sources, such as atmospheric and multipath effects, are correlated with elevation
 213 angle. In general, they monotonically increase as elevation angle decreases as described in the
 214 conventional elevation angle based weighting model (Special-Committee-159 2001). Figure 7
 215 shows the relationship between NLOS delay with elevation angle. It is clear that the NLOS
 216 decreases as the elevation increases, in the other words, using the conventional elevation model
 217 in weighted LSE is also able to mitigate the NLOS effect. As shown in the figure, when the
 218 elevation angle is between 10 to 20 degree, its C/N_0 is usually lower than 30 dB-Hz. This
 219 phenomenon proves the agreement that both applying C/N_0 or elevation angle based weighting
 220 models can improve GPS positioning when NLOS signal is present. However, it is not necessary
 221 that the lower the elevation angle is, the lower the carrier to noise ratio is. Figure 8 shows the
 222 different behaviors between the received signal strength of LOS and NLOS using the same
 223 commercial GNSS receiver. As shown in the figure, the mean of C/N_0 of LOS increases as the
 224 elevation increases. Its standard deviation decreases as the elevation increases. In the other words,
 225 the quality of LOS is more stable at higher elevation angle. The NLOS data shows a very

226 different behavior. As the elevation increases, the C/N_0 does not increase following the behavior
227 shown in the data of LOS. The standard deviation of NLOS C/N_0 also does not show the obvious
228 tendency with elevation variation. The reason is that the NLOS is a reflected signal. The
229 material of the reflecting surface can greatly change the signal strength of reflected signals.
230 Comparing the top and bottom panels, one might conclude that C/N_0 could be used to distinguish
231 the LOS or NLOS signal as the elevation angle increase. This conclusion is similar to the finding
232 in Yozevitch et al. (2016) on LOS/NLOS classification using machine learning approach.

233



234

235 **Fig. 7** NLOS pseudorange error with respect to elevation angle of the 24-hours data. The color
236 denotes the carrier to noise ratio of each point.

237

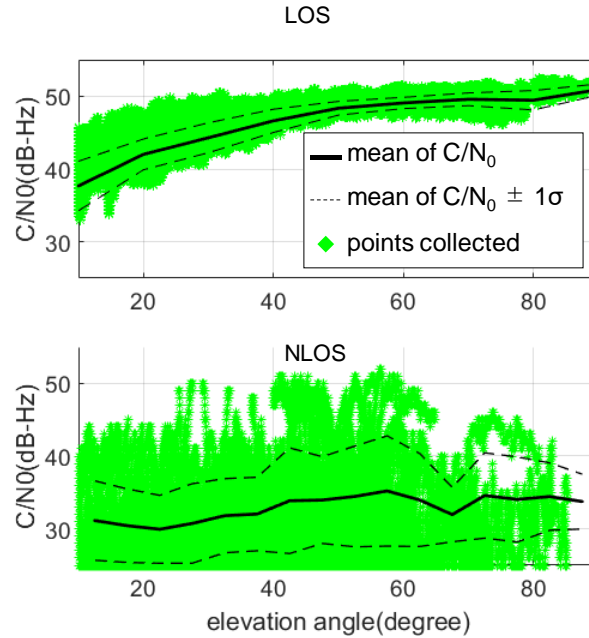


Fig. 8 Comparison of LOS and NLOS in terms of C/N_0 with regards to elevation.

238
239
240

241 The statistic of a large amount of data can reveal the general characteristic of NLOS delay.
242 It will be interesting to study whether short data would comply with the summarized
243 characteristics or not.

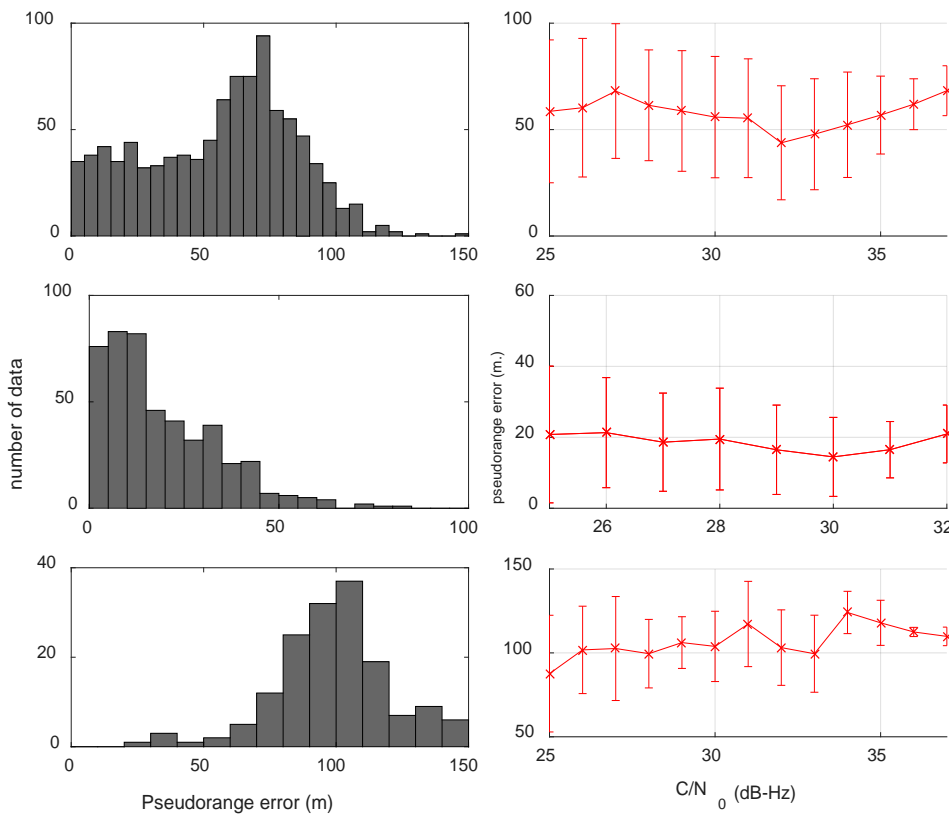
244

245 NLOS data 2: Case of 30 minutes

246 In the 30-minutes data, there are 1,648 NLOS measurements detected from 3 different satellites
247 as shown in the bottom panel of Figure 4. There are 4 LOS, 3 NLOS and 1 multipath signal in
248 this case. Similar analysis is conducted to the 30-minutes data as shown in Figures 9 and 10. To
249 observe Figure 9, the NLOS pseudorange delay does not decrease as the C/N_0 increases. Instead,
250 it remains a similar delay with different C/N_0 . Interestingly, the pseudorange delay is still
251 correlated with the elevation angle as shown in Figure 10, namely, the higher elevation angle, the
252 smaller the NLOS pseudorange. Based on the principle of the GPS signal tracking loop, the
253 effect of NLOS is different from multipath. For NLOS, only the delayed (reflected) signals
254 comes in to the receiver, which could easily deceive the receiver that the NLOS signal is LOS
255 signal. According to the algorithm of estimating C/N_0 (Sharawi et al. 2007), the carrier strength
256 is calculated by accumulating the power of I and Q channels. If NLOS signal are continuously
257 present in the environment, its C/N_0 could also be strong. Thus, the strong C/N_0 is not necessary

258 indicating a clean measurement. It could still contain tens of meters of pseudorange error. The
 259 previously obtained characteristic from the 2- hours data of NLOS delay varying with C/N_0 is
 260 due to the C/N_0 being correlated with the elevation angle. In fact, C/N_0 could increase as the
 261 elevation angle increased because of the longer signal transmission path and the pattern of
 262 antenna gain. As a result, it can be concluded that elevation angle is a dominant factor to NLOS
 263 pseudorange errors.

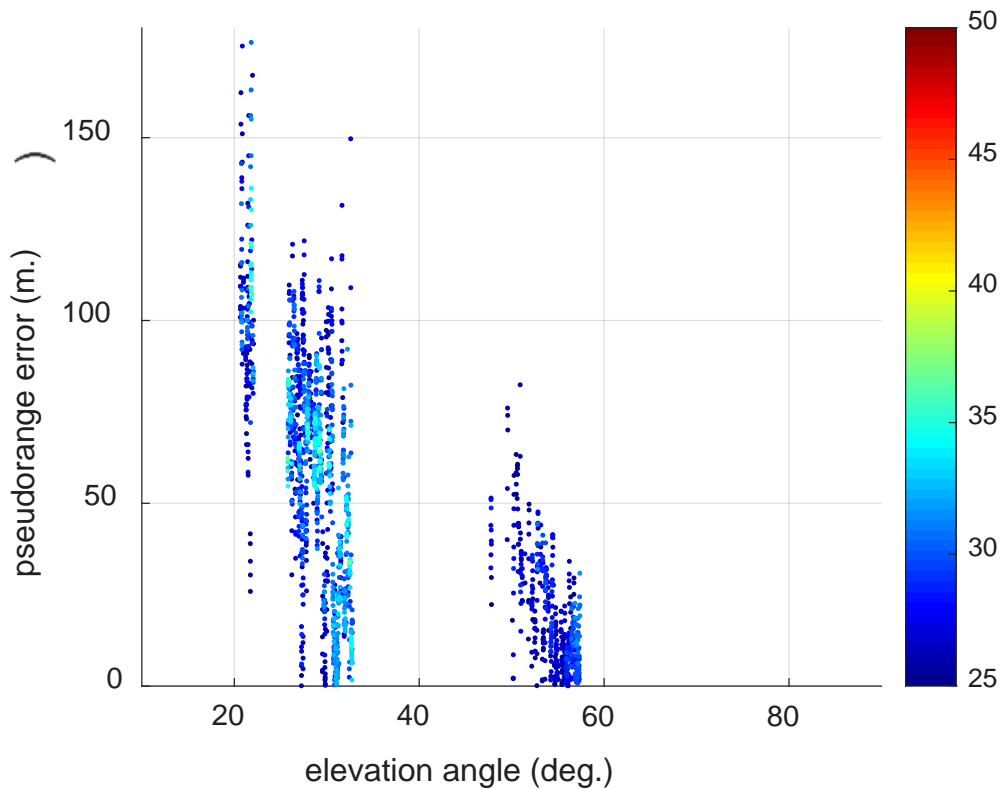
264



265

266 **Fig. 9** Three NLOS signals from different satellite are collected. Left panel denotes histogram of
 267 NLOS delay and right panel denotes mean and standard deviation of NLOS pseudorange error
 268 with respect to carrier to noise ratio of the 30-minutes data.

269



270

271 **Fig. 10** NLOS pseudorange error with respect to elevation angle of the 30-minutes data. The
 272 color denotes the carrier to noise ratio of each point.

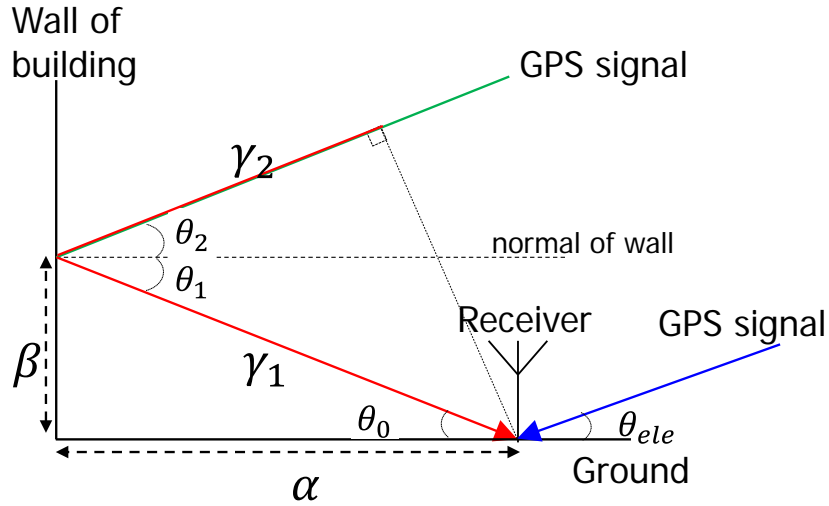
273

274 **Modelling of NLOS**

275 This section tries to derive a model to represent NLOS delay using the dominant factor, i.e. the
 276 elevation angle, previously verified. In highly-urbanized areas, most of the buildings use
 277 excessive glass windows as a face of modern architecture. We, therefore, assume the GPS signal
 278 reflection follows the law of reflection to model the NLOS signal. An illustration of a perfect
 279 reflecting signal received by a receiver is given in Figure 11.

280

281



282

283

Fig. 11 Illustration of a reflecting signal that followed the law of reflection.

284

285 The blue line represents a LOS signal. Green and red lines are the reflecting signal. Due to the
 286 distance between satellite and receiver is large compared to the distance between the LOS and
 287 reflecting signals, the blue line is not only parallel to the greens but also same length. Therefore,
 288 the NLOS delay (γ) in the pseudorange domain is the red lines:

289
$$\gamma = \gamma_1 + \gamma_2 \tag{6}$$

290 where γ_1 and γ_2 are:

291
$$\gamma_1 = \alpha \sec \theta_0 \tag{7}$$

292
$$\gamma_2 = \gamma_1 \cos(\theta_1 + \theta_2) \tag{8}$$

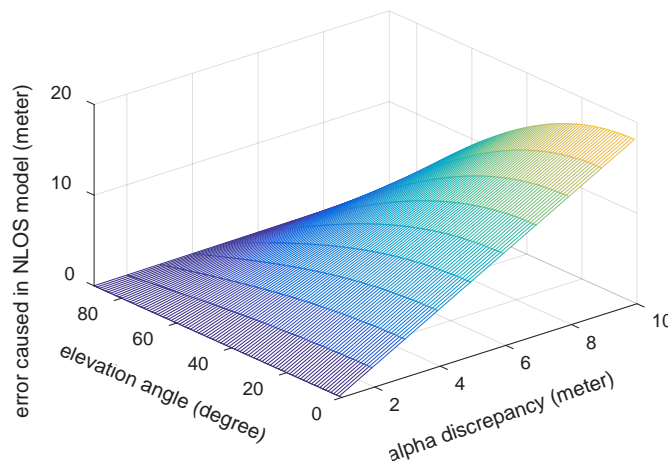
293 where α denotes the distance between the receiver to the obstacles (buildings) that reflected the
 294 navigation signal. Angle of reflection θ_1 equals to the angle of incidence θ_2 because the law of
 295 reflection is assumed. In addition, since the green and blue lines are parallel, θ_1 and θ_0 are
 296 alternate interior angles, namely, $\theta_1 = \theta_0$. Assuming the wall of building is perpendicular to the
 297 ground, thus the normal of wall is parallel to ground resulting $\theta_2 = \theta_{ele}$. θ_{ele} denotes the
 298 elevation angle of the satellite. Finally, $\theta_{ele} = \theta_2 = \theta_1 = \theta_0$, thus the NLOS delay can be
 299 represented as:

300
$$\gamma = \alpha \sec \theta_{ele} (1 + \cos 2\theta_{ele}) \tag{9}$$

301 In (9), only the distance between the receiver to the obstacle is unknown to a GPS receiver.
302 Fortunately, this distance α could be roughly obtained from the 2D maps that are widely
303 available to vehicle navigator and pedestrian with smartphone. According to road planning
304 standards and guidelines of HK government, the general road width for primary and district
305 distributor is between 6.75 to 13.5 m (HKPSG 2016). The path width of pedestrian walk is
306 between 3.5 to 4.5 m (HKPSG 2016). Thus, a proper value of α in HK will be from 3.5 to 18 m
307 for vehicle applications. For the autonomous driving, the LiDAR sensor will provide the
308 distances between vehicle and buildings, which can be used by the proposed NLOS model.

309 Considering an example, the alpha will be set to 18.2 meters based on the map information, but
310 alpha measured by LiDAR is 15.6 meters. In the case of elevation angle of 61.6 degrees and the
311 alpha discrepancy of 2.6 m, the error introduced to the proposed NLOS model is 2.5 m. To
312 further discuss other cases, a simulation of error introduced under different elevation angle and
313 alpha discrepancy is shown in Figure 12. As can be seen, the newly introduced error is smaller
314 the higher of elevation angle and smaller the alpha discrepancy.

315



316

317 **Fig. 12** Pseudorange error caused in the proposed NLOS model if alpha is not accurate.

318

319

320 Experiment Result

321 A commercial GPS receiver, u-blox M8, is deployed to collect NLOS data. Two different
322 locations at a highly urbanized city are selected to evaluate the performance of the proposed
323 NLOS model in pseudorange and position domains, respectively.

324

325 Verification of the NLOS model in pseudorange domain

326 In order to evaluate the proposed model in different elevation angle, a long-time data with NLOS
327 signal must be collected. Figure 13 demonstrates the environment that the data was collected.
328 The antenna is attached with a stick and put outside of the window for long time data collection.

329



330

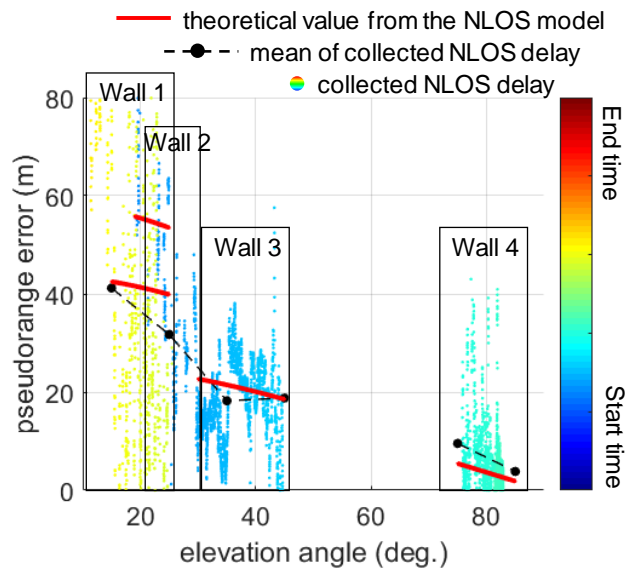
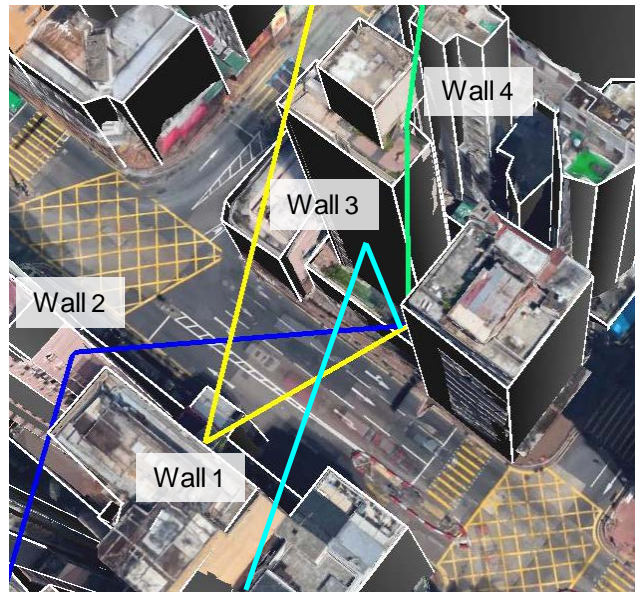
331 **Fig. 13** NLOS can be frequently observed in typical urban residential area in Asian urbanized
332 city. The left panel denotes the environment of the data was collected and right panel indicate the
333 installment of the path antenna.

334

335 Figure 14 shows an example that the NLOS signal from a same satellite that travelled
336 from 0 to 85 degree of elevation angle.

337

338



339

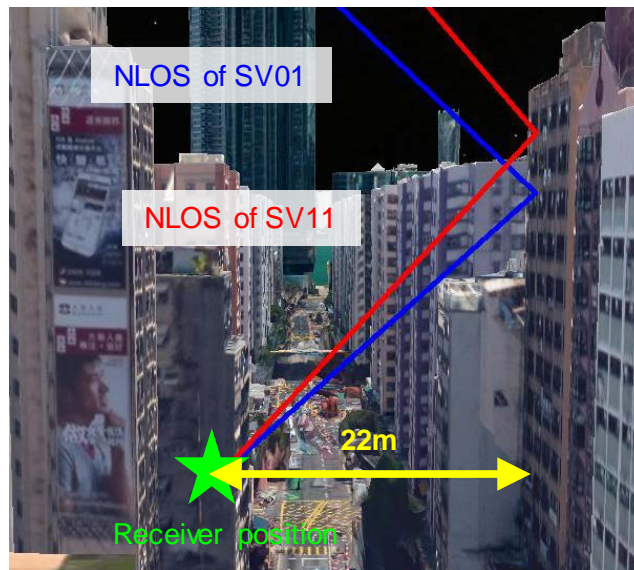
340 **Fig. 14** Example of a received NLOS signal. Top panel demonstrates signal traveling paths
341 reflected at 4 different walls by ray-tracing simulation, and bottom panel shows the NLOS delay
342 of SV 27 that traveled from 0 to 85 degrees of elevation angle.

343

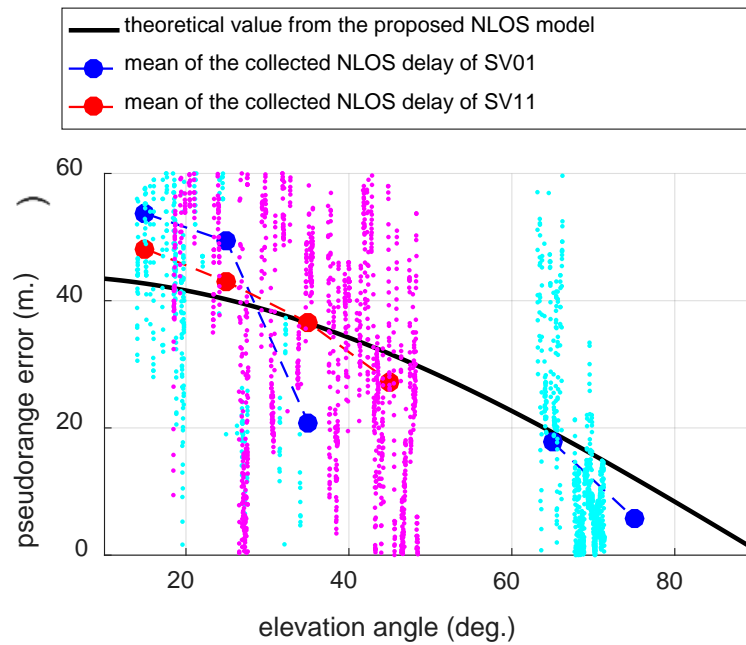
344 The x-axis of the bottom panel of Figure 14 is the elevation angle of measurement, and the
345 y-axis is the NLOS delay in pseudorange domain calculated by (5). The black dashed line
346 denotes the mean of the collected NLOS delay of different elevation angle (with a resolution of
347 10 degree). The trend of the collected NLOS delay decreases as the elevation increases. It is clear

348 that the signal transmission path of SV 27 was not blocked during the elevation angle between 45
349 to 75 degrees as shown in the bottom panel. The color of each point denotes the time of
350 recording data, the bluer the point is earlier that signal is collected. The NLOS reflections of SV
351 27 are caused by four different buildings as shown in the top panel. Thus, the NLOS delays can
352 be separated into four different groups. The red solid lines of the bottom panel denote the
353 theoretical NLOS delay calculated from the proposed model. The distances between the receiver
354 and the walls (α) are about 22, 29.5, 13.1 and 10.5 m for Wall 1 to 4, respectively. As can be seen
355 from the bottom panel, the theoretical values are similar to the mean of collected values (with a
356 region of 10 meters), expecting reflection from Wall 2. In fact, during the elevation angle from
357 20 to 30 degrees, the receiver has a great possibility to receive multiple NLOS signals
358 simultaneously. This effect is called *multipathing NLOS*, which is complicated to model due to
359 the undisclosed tracking correlator design of commercial receiver. To better verify the proposed
360 model, signals reflected at the same wall but from different satellites are preferred. Most of the
361 reflections of the long-time collected data comes from Wall 1 shown in the top panel.

362



363



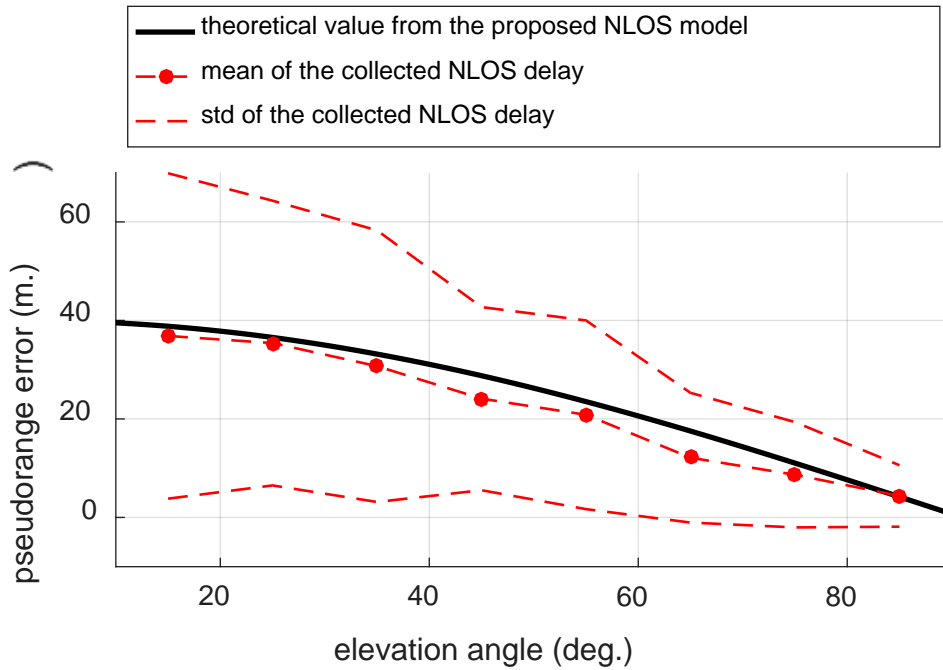
364

365 **Fig. 15** Example of the two received NLOS signals reflected at same building. Top panel shows
 366 the ray-tracing simulation of NLOS from SV01 and SV11 reflected at Wall 1. Bottom panel
 367 shows the collected NLOS delay and theoretical value calculated by the proposed model.

368

369 Figure 15 shows the cases of the other two satellites, SV01 and SV11, that only reflected at
 370 Wall 1. The black solid line of bottom panel denotes the NLOS delay calculated from the
 371 proposed model. Even through the data is noisy, the mean of NLOS delay is still close to the
 372 proposed model. This result verifies that if the NLOS is a single refecton from a wall, the
 373 proposed model can predict the NLOS delay. All the NLOS reflected at Wall 1 from different
 374 SVs is organized in Figure 16.

375



376

377 **Fig. 16** Mean and standard deviation of all the NLOS delays reflected at Wall 1 from different
 378 SVs.

379

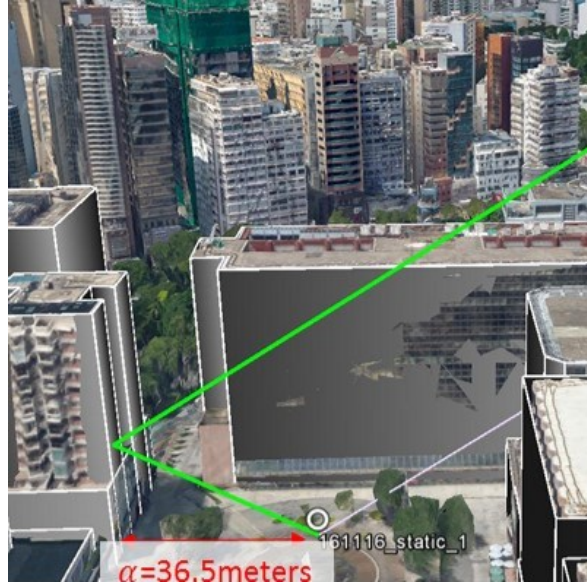
380 The theoretical value calculated from the proposed NLOS model, namely (9), is very close
 381 to the mean of the data. In the other words, the proposed method can obtain the mean of NLOS
 382 but not the standard deviation. Interestingly, the standard deviation of the data decreases as the
 383 elevation angle increases because the lower the elevation angle is, the lower the C/N_0 is
 384 obtained.

385

386 Positioning method using hypothesis-based positioning method

387 A static experiment is conducted in the environment shown in the Figure 17. Many glassy
 388 buildings are surrounded to the receiver. A measurement with NLOS reflection is detected and
 389 simulated in the figure. The distance between the building and receiver is about 36.5 meters.

390



391

392

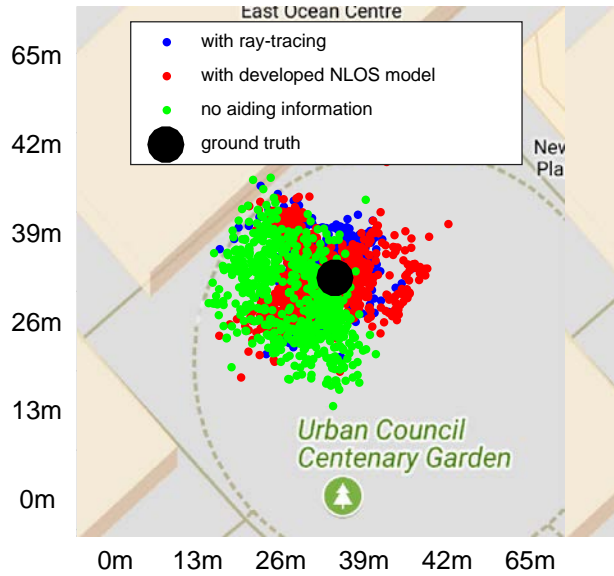
Fig. 17 Ray-tracing simulation of the static experiment.

393

394 To apply the proposed NLOS model, the position of receiver is essential. The previous work
 395 proposes a position hypothesis-based positioning method (Hsu et al. 2016b). This approach
 396 distributes several position candidates and gives them proper weighting by evaluating their
 397 pseudorange similarities between the ray-tracing results and measurements. This positioning
 398 method is used to evaluate the NLOS model proposed. The NLOS pseudorange delay based on
 399 ray-tracing is replaced as the NLOS model. The rest of algorithm is the same. The positioning
 400 results of the hypothesis method using ray-tracing, the NLOS and without any aiding information
 401 is demonstrated and evaluated in Figure 18 and Table 1. Only the data with the identified NLOS
 402 measurement is evaluated. It is important to note that NLOS identification is required in the
 403 hypothesis-based positioning method. The three methods evaluated above used 3D building
 404 models to determine the signal type of each measurements. It is evident that the method with ray-
 405 tracing simulation certainly obtained the best performance among the three methods, which is
 406 about 5 meters of horizontal positioning accuracy. However, its computational load is also much
 407 higher than that of the other two. The hypothesis-based method using the proposed NLOS model
 408 achieve 6.27 meters of accuracy, which is slightly worse than the method with ray-tracing. If no
 409 any aiding information used to correct the NLOS measurements, the positioning accuracy is
 410 about 8.67 meters. This result verifies the proposed NLOS model is capable of replacing the use

411 of ray-tracing in calculating NLOS delay in the pseudorange domain.

412



413

414 **Fig. 18** Result of hypothesis based positioning method using 3D building mode, the proposed
415 NLOS model and no aiding information.

416

417 **Table 1** Positioning performance of hypothesis based positioning method using ray-tracing, the
418 proposed NLOS model and no aiding information.

Methods	Mean (meter)	Standard deviation (meter)
Ray-tracing	5.05	2.99
Proposed NLOS model	6.27	3.31
No aiding information	8.67	3.93

419

420 Conclusions and Future Work

421 Multipath interference and NLOS reception are major error sources when using GNSS
422 positioning in urban environments. We first analyze a long-time GPS NLOS data and
423 summarizes as follows 1) The NLOS delay is not fitted to Gaussian distribution. Instead, it is

424 more similar to a gamma distribution; 2) Mitigating NLOS effects by given weighting based on
425 C/N_0 could be incorrect; 3) NLOS delay is highly correlated to the elevation angle. The second
426 contribution is to propose an innovative NLOS model. The NLOS model is based on the
427 elevation angle and the distance between the receiver and the building that reflected the NLOS
428 signal. If the distance can be appropriately selected, the proposed model can accurately describe
429 the NLOS delay of the measurements. The effectiveness of the proposed model is demonstrated
430 by applying it into a hypothesis based positioning algorithm. The experiment result shows the
431 positioning error only to increase about 1.3 meter after replacing the NLOS delay, estimated by
432 ray-tracing, into the proposed model in the particle filter based positioning algorithm.

433 However, this result still applies the ray-tracing to identify whether the measurement is
434 LOS or NLOS. Concerning the practical use of the proposed NLOS model, it requires working
435 with other NLOS detection algorithms. To reduce the computational load, we provide three
436 suggestions to integrate with the proposed NLOS model. 1) Using additional memory space: an
437 ideal approach is to integrate the proposed NLOS model with shadow matching positioning
438 algorithm (Groves 2011), which only applies the building boundary (using only memory). 2)
439 Benefiting from Big Data era: Another promising and innovative approach is to implement
440 LOS/NLOS classifier trained by unsupervised/supervised machine learning algorithm before
441 applying the proposed NLOS model. As suggested in Yozevitch et al. (2016), their decision tree
442 based robust classifier achieves over 85% of accuracy of NLOS detection. 3) Increasing the
443 instrument cost: Alternatively, a dual-polarization antenna can be implemented in the localization
444 system to effectively detect NLOS reception (Jiang and Groves 2014).

445 An interesting future work could be modeling the residue of multipath effect after
446 applying sophisticated correlator design. The nature of multipath effect is very different with
447 NLOS reception. To study the multipath residue, a software receiver is required to take the
448 advantage of its flexibility to alter the correlator design of code tracking loop.

449

450 **Reference**

451 Ahmad KAB, Sahmoudi M, Macabiau C, Bourdeau A, Moura G (2013) Reliable GNSS
452 Positioning in Mixed LOS/NLOS Environments Using a 3D Model. In: European
453 Navigation Conference (ENC), Vienne, Austria, April 2013, 1-9.

454 Benson D (2007) Interference Benefits of a Vector Delay Lock Loop (VDLL) GPS Receiver.
455 Proc. ION AM 2007, Institute of Navigation, Cambridge, Massachusetts, USA, April 23-
456 25, 749-756.

457 Betaille D, Peyret F, Ortiz M, Miquel S, Fontenay L (2013) A New Modeling Based on Urban
458 Trenches to Improve GNSS Positioning Quality of Service in Cities IEEE Intelligent
459 Transportation Systems Magazine 5:59-70

460 Blanch J, Walter T, Enge P (2015) Fast Multiple Fault Exclusion with a Large Number of
461 Measurements. Proc. ION ITM 2015, Dana Point, California, USA, January 26-28, 2015,
462 696-701.

463 Breßler J, Reisdorf P, Obst M, Wanielik G GNSS positioning in non-line-of-sight context-a
464 survey. In: 2016 IEEE 19th International Conference on Intelligent Transportation
465 Systems (ITSC), 1-4 Nov. 2016. pp 1147-1154.

466 Chiang K-W, Duong T, Liao J-K (2013) The Performance Analysis of a Real-Time Integrated
467 INS/GPS Vehicle Navigation System with Abnormal GPS Measurement Elimination
468 Sensors 13:10599-10622

469 Groves PD (2011) Shadow Matching: A New GNSS Positioning Technique for Urban Canyons
470 The Journal of Navigation 64:417-430 doi: 10.1017/S0373463311000087

471 Groves PD (2013) Principles of GNSS, Inertial, and Multi-Sensor Integrated Navigation Systems
472 (GNSS Technology and Applications). 2nd edn. Artech House Publishers,

473 Groves PD, Jiang Z (2013) Height Aiding, C/N 0 Weighting and Consistency Checking for
474 GNSS NLOS and Multipath Mitigation in Urban Areas The Journal of Navigation
475 66:653-669

476 Groves PD, Wang L, Adjrad M, Ellul C GNSS Shadow Matching: The Challenges Ahead. In:
477 Proceedings of ION GNSS+ 2015, Tampa, Florida, Sept. 2015. pp 2421-2443

478 Gu Y, Hsu L-T, Kamijo S (2015) GNSS/On-Board Inertial Sensor Integration with the Aid of 3D
479 Building Map for Lane-Level Vehicle Self-Localization in Urban Canyon Vehicular
480 Technology, IEEE Transactions on 65:4274-4287

481 Han H, Wang J, Wang J, Tan X (2015) Performance Analysis on Carrier Phase-Based Tightly-

482 Coupled GPS/BDS/INS Integration in GNSS Degraded and Denied Environments
483 Sensors 15:8685

484 Hartinger H, Brunner FK (1999) Variances of GPS Phase Observations: The SIGMA- ϵ Model
485 GPS Solutions 2(4):35-43

486 HKPSG (2016) Hong Kong Planning Standards and Guidelines. Technical Services Section of
487 Planning Department, Government of Hong Kong

488 Hsu L-T, Gu Y, Huang Y, Kamijo S (2016a) Urban Pedestrian Navigation using Smartphone-
489 based Dead Reckoning and 3D Maps Aided GNSS Sensors Journal, IEEE 16:1281-1293

490 Hsu L-T, Gu Y, Kamijo S (2016b) 3D building model-based pedestrian positioning method using
491 GPS/GLONASS/QZSS and its reliability calculation GPS Solutions 20:413–428

492 Hsu L-T, Jan S-S, Groves P, Kubo N (2015) Multipath mitigation and NLOS detection using
493 vector tracking in urban environments GPS Solutions 19:249-262

494 Hsu L-T, Tokura H, Kubo N, Gu Y, Kamijo S (2017) Multiple Faulty GNSS Measurement
495 Exclusion based on Consistency Check in Urban Canyons IEEE Sensors Journal,
496 17(6):1909-1917

497 Isaacs JT, Irish AT, Quitin F, Madhow U, Hespanha JP Bayesian localization and mapping using
498 GNSS SNR measurements. In: 2014 IEEE/ION Position, Location and Navigation
499 Symposium - PLANS 2014, 5-8 May 2014. pp 445-451.

500 Iwase T, Suzuki N, Watanabe Y (2013) Estimation and exclusion of multipath range error for
501 robust positioning GPS Solutions 17:53-62

502 Jiang Z, Groves P (2014) NLOS GPS signal detection using a dual-polarisation antenna GPS
503 Solutions 18:15-26

504 Kanwal N, Hurskainen H, Nurmi J (2010) Vector tracking loop design for degraded signal
505 environment. Ubiquitous Positioning Indoor Navigation and Location Based Service,
506 Kirkkonummi, Finland, October 14-15, 2010, 1-4.

507 Kumar R, Petovello MG (2014) A Novel GNSS Positioning Technique for Improved Accuracy in
508 Urban Canyon Scenarios Using 3D City Model. Proc. ION GNSS+ 2014, Tampa,
509 Florida, USA, September 8-12, 2014, 2139-2148.

510 Li B, Cui W, Wang B (2015) A Robust Wireless Sensor Network Localization Algorithm in
511 Mixed LOS/NLOS Scenario Sensors 15:23536

512 Misra P, Enge P (2011) Global Positioning System: Signals, Measurements, and Performance.
513 Ganga-Jamuna Press, Lincoln, MA 01773

514 Miura S, Hsu LT, Chen F, Kamijo S (2015) GPS Error Correction With Pseudorange Evaluation
515 Using Three-Dimensional Maps Intelligent Transportation Systems, IEEE Transactions
516 on 16:3104 - 3115

517 Peyraud S, Bétaille D, Renault S, Ortiz M, Mougel F, Meizel D, Peyret F (2013) About Non-
518 Line-Of-Sight Satellite Detection and Exclusion in a 3D Map-Aided Localization
519 Algorithm Sensors 13:829-847

520 Peyret F, Bétaille D, Carolina P, Toledo-Moreo R, Gómez-Skarmeta AF, Ortiz M (2014) GNSS
521 Autonomous Localization: NLOS Satellite Detection Based on 3-D Maps IEEE Robotics
522 & Automation Magazine 21:57-63

523 Sharawi MS, Akos DM, Aloï DN (2007) GPS C/N0 estimation in the presence of interference
524 and limited quantization levels Aerospace and Electronic Systems, IEEE Transactions on
525 43:227-238

526 Special-Committee-159 (2001) Minimum Operational Performance Standards for Global
527 Positioning System/Wide Area Augmentation System Airborne Equipment Document,
528 DO-229C, RTCA

529 Sun D, Petovello MG, Cannon ME (2013) Ultratight GPS/Reduced-IMU Integration for Land
530 Vehicle Navigation IEEE Transactions on Aerospace and Electronic Systems 49:1781-
531 1791

532 Suzuki T, Kubo N (2013) Correcting GNSS Multipath Errors Using a 3D Surface Model and
533 Particle Filter. Proc. ION GNSS+ 2013, Nashville, Tennessee, USA, September 16-20,
534 2013, 1583-1595.

535 Veitsel VA, Zhdanov AV, Zhodzishsky MI (1998) The Mitigation of Multipath Errors by Strobe
536 Correlators in GPS/GLONASS Receivers GPS Solutions 2:38-45

537 Wang JH, Gao Y (2010) Land Vehicle Dynamics-Aided Inertial Navigation IEEE Transactions

538 on Aerospace and Electronic Systems 46:1638-1653

539 Wang L, Groves P, Ziebart M (2012) Multi-Constellation GNSS Performance Evaluation for
540 Urban Canyons Using Large Virtual Reality City Models. *Journal of Navigation* 65:459-
541 476

542 Wang L, Groves PD, Ziebart MK (2013) GNSS Shadow Matching: Improving Urban Positioning
543 Accuracy Using a 3D City Model with Optimized Visibility Scoring Scheme. *Navigation*,
544 60:195-207

545 Wang L, Groves PD, Ziebart MK (2015) Smartphone Shadow Matching for Better Cross-street
546 GNSS Positioning in Urban Environments. *Journal of Navigation* 68:411-433

547 Yozevitch R, Ben-Moshe B, Dvir A (2014) GNSS Accuracy Improvement Using Rapid Shadow
548 Transitions *IEEE Transactions on Intelligent Transportation Systems* 15:1113-1122

549 Yozevitch R, Ben-Moshe B (2015) A Robust Shadow Matching Algorithm for GNSS Positioning
550 *Navigation* 62:95-109

551 Yozevitch R, Ben-Moshe B, Weissman A (2016) A Robust GNSS LOS/NLOS Signal Classifier.
552 *Navigation* 63:429-442

553 Zhdanov A, Zhodzishsky M, Veitsel V, Ashjaee J (2002) Evolution of Multipath Error Reduction
554 with Signal Processing. *GPS Solutions* 5:19-28

555

556 **Author Biographies**

557 Li-Ta Hsu received the B.S. and Ph.D. degrees in aeronautics and astronautics from National
558 Cheng Kung University, Taiwan, in 2007 and 2013, respectively. He is currently an assistant
559 professor with Interdisciplinary Division of Aeronautical and Aviation Engineering, The Hong
560 Kong Polytechnic University, before he served as post-doctoral researcher in Institute of
561 Industrial Science at University of Tokyo, Japan. In 2012, he was a visiting scholar in University
562 College London, U.K. His research interests include GNSS positioning in challenging
563 environments and localization for autonomous driving vehicle and unmanned aerial vehicle.